

Comparative study between PI and SMC controllers for DFIG using fuzzy wind power estimator

Atef Jemmali, Khaled Elleuch, Hafedh Abid, Ahmed Toumi

Laboratory of Sciences and Techniques of Automatic Control and Computer Engineering (Lab-STA),
Department of Electrical Engineering, National School of Engineering of Sfax, University of Sfax, Sfax, Tunisia

Article Info

Article history:

Received Jan 31, 2023

Revised Mar 14, 2023

Accepted Mar 29, 2023

Keywords:

DFIG

Doubly-fed

PI controllers

SMC

Wind turbine

ABSTRACT

In this paper, we are interested in the control of the rotor current of the doubly feed induction generator (DFIG), that is used in wind turbines. In this context, we present a comparative study between two types of controllers. The first is based on a classic PI proportional-integral control, while the second is based on the SMC sliding control. The command chain uses a fuzzy estimator of the wind power, which makes it possible to determine the reference speed of DFIG. The system includes essentially a turbine, two converters, one on the rotor side and the other on the grid side, and a filter. The grid-side converter is used to maintain a constant DC bus voltage and to control rotor reactive power. The rotor side converter is used to control the speed of the DFIG to guarantee maximum power extracted from the turbine. In addition, this converter allows controlling the reactive power through the control of the rotor current according to the axis "d" of the frame linked to the rotating field. The simulation results show the effectiveness of sliding mode control (SMC) for the considered system.

This is an open access article under the [CC BY-SA](https://creativecommons.org/licenses/by-sa/4.0/) license.



Corresponding Author:

Atef Jemmali

Laboratory of Sciences and Techniques of Automatic Control and Computer Engineering (Lab-STA)

Department of Electrical Engineering, National School of Engineering of Sfax, University of Sfax

Sfax, Tunisia

Email: atefjemmali@gmail.com

1. INTRODUCTION

Wind power is one of the main sources of energy used by humanity. Indeed, it is known as a clean renewable energy and it is free. The popular development in the world and the growing needs for electrical energy in the industrial and domestic fields has led to think of other sources of energy such as renewable energy which has several advantages [1], [2]. After the recurrent global oil crises, the exploitation and installation of wind energy sources are increasingly recommended and encouraged. Indeed, there are two main configurations of wind turbines. The first configuration, which does not use static energy converters, operates at a fixed speed. While the second configuration, which uses static converters installed between the generator and the network, operates at variable speed. This last configuration allows wind energy to be converted at different wind speeds.

In wind systems, several types of generators are used such as the permanent magnet synchronous generator (PMSG), the asynchronous machine and the double-feed induction machine [3]. In the literature of wind energy system (WES), several large-power wind turbines installed in the world use the doubly-feed induction-generator (DFIG). This latest, presents an advantage in the production levels of electrical energy for variable speeds, which can reach 30% of synchronism speed, hence a significant range of wind speed is exploited [4]. The control strategy of DFIG consists of keeping the DC bus voltage constant and controlling

the rotor active power through the control of the rotor current according to the quadratic axis of the rotating frame of reference. The DC bus is located between two converters. The last converter is followed by an (L, r) type filter [5], [6].

The control of DFIG is based on the orientation of the flux of the stator in the two-phase reference (d, q) according to the axis d which leads to the decoupling of the quantities between the two axes d and q of the rotor [7]–[9]. In the literature of wind energy conversion system (WECS) using DFIG, several control techniques are proposed. One of the best-known methods are the classic proportional integral (PI) controller [10], [11]. A linear quadratic regulator (LQR) controller is used to control the DFIG based WES as shown in [12]. This controller giving stability but it can lose this due to variations of parameters or operating point. So, to obtain a robust control, a sub-optimal H_∞ regulator was used. The work in [13] describes a nonlinear model predictive control (NMPC) that is presented to a WECS based on DFIG. The strategy consists to use torque-current control loop engender the rotor reference voltage and speed control loop that yields the reference of the torque. The works in [14]–[16] explain how sliding mode control (SMC) is used to change the inner current loop of the conventional vector control. The gains of control are chosen using positive semi-definite barrier function to evade chattering effect. Fuzzy logic control constitutes an approach used by several researchers. Indeed, this approach can give robust regulators to the change of parameters machine or grid, the fuzzy regulators can be developed without need of the mathematical model system, it is enough to know the dynamic behavior [17]. Despite the effectiveness of these controllers, they remain complex especially at the implementation. SMC approach combined with fuzzy logic control is applied to control a variable speed of WECS using DFIG [18]. The adaptive neuro-fuzzy inference system uses maximum power point tracking controller for DFIG based WECS [19]. This approach resulted in less chatter compared to the conventional PI controller for a wide wind range.

The main contribution consists to use a new sliding mode control, which has the same structure as the proportional-integral controller. Also, the paper includes a comparative study between the integral proportional controllers with that of the proposed sliding mode. A fuzzy supervisor of the T-S type is used to predict the optimal speed of the turbine, which allows extracting the maximum energy from the wind.

This paper is organized as follows: The first part of the next section describes WECS based on DFIG. Then, the second and third parts respectively present mathematical models of the turbine and the DFIG. The control strategy is described in section 3. Indeed, the first part is reserved to the presentation of the classical PI control strategy applied to the DFIG. The second part is concerned to the elaboration of control law basis on SMC. While the third part describes the new T-S fuzzy supervisor. This latest allows predicting, at any time and wind speed, the optimal speed for the turbine to extract the maximum energy from wind. Discussions and simulation results are shown in section 4. Then, the paper is closed by a conclusion.

2. MODEL OF WIND ENERGY CONVERSION SYSTEM

2.1. System description

The system contains essentially a turbine, two converters and a filter. The first converter controls the operating point of DFIG, while the second AC/DC converter is used to keep constant the DC bus voltage and to control both the active and reactive rotor powers injected to the electrical grid. In this structure, the wind turbine rotates with variable speed. The rotor side converter is used to control the speed of the DFIG to guarantee maximum power extracted from the turbine. The structure of connections with the grid is displayed in the Figure 1 [20], where RSC and GSC stand for rotor side converter and grid side converter respectively.

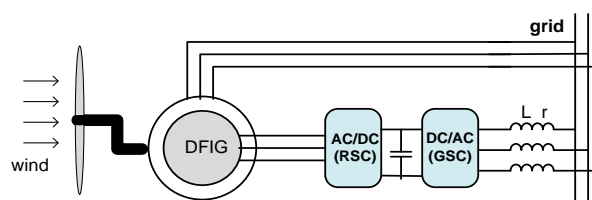


Figure 1. General architecture of wind energy plant based on DFIG

2.2. Model of wind turbine

It is well known that a Wind Turbine transforms wind energy into mechanical energy on the shaft of the DFIG using a speed reducer. The power at the turbine shaft can be written according to the following formula [21], [22]:

$$P_a = \frac{1}{2} \pi \rho v^3 R^2 C_p(\lambda, \beta) \quad (1)$$

with:

$$\lambda = \frac{R\Omega_t}{v} \quad (2)$$

Where C_p , β , λ , Ω_t , R , ρ and v define respectively power coefficient, pitch angle, tip-speed-ratio, turbine speed, radius of the turbine, air density and wind speed. Each turbine is defined by its own power coefficient which is limited by a maximum power called the Betz limit equal to 0.59. The following Figure 2. Shows the evolution of C_p as a function of λ .

2.3. DFIG model

The most standard structures of WECS use the DFIG, as shown in Figure2. In this case, the turbine is linked to DFIG through a gearbox [23]. By transforming the inertia and the viscous friction of the turbine to the DFIG, the global mechanical dynamics of the rotor is written as follows:

$$J \frac{d\Omega}{dt} + f\Omega = \Gamma_a - \Gamma_g \quad (3)$$

where, J: total inertia of the wind turbine, Γ_a : electromagnetic torque of the DFIG, f : total coefficient of viscous friction of the turbine and Γ_g : turbine mechanical torque on the shaft of the machine. The electrical dynamic model of the DFIG is described in the d-q rotating synchronous frame. The equations voltage of stator and rotor are given respectively by (4) and (5):

$$\begin{cases} V_{ds} = R_s I_{ds} + \dot{\psi}_{ds} - \omega_s \psi_{qs} \\ V_{qs} = R_s I_{qs} + \dot{\psi}_{qs} + \omega_s \psi_{ds} \end{cases} \quad (4)$$

$$\begin{cases} V_{dr} = R_r I_{dr} + \dot{\psi}_{dr} - (\omega_s - \omega_r) \psi_{qs} \\ V_{qr} = R_r I_{qr} + \dot{\psi}_{qr} + (\omega_s - \omega_r) \psi_{ds} \end{cases} \quad (5)$$

The ω_s and ω_r are respectively the pulsations of the stator and rotor currents. I_{ds}, I_{qs}, I_{dr} and I_{qr} represent respectively the stator and rotor currents. R_s and R_r represent respectively the stator and rotor windings resistances. The expressions of the stator and rotor fluxes are written as (6) and (7).

$$\begin{cases} \psi_{ds} = L_s I_{ds} + M_{sr} I_{dr} \\ \psi_{qs} = L_s I_{qs} + M_{sr} I_{qr} \end{cases} \quad (6)$$

$$\begin{cases} \psi_{dr} = L_r I_{dr} + M_{sr} I_{ds} \\ \psi_{qr} = L_r I_{qr} + M_{sr} I_{qs} \end{cases} \quad (7)$$

L_s , L_r and M_{sr} represent respectively the inductances of the stator, the rotor and the mutual. The expression of the electromagnetic torque is written as (8).

$$\Gamma_a = n_p \frac{M_{sr}}{L_s} (I_{dr} \psi_{qs} - I_{qr} \psi_{ds}) \quad (8)$$

The n_p denote the pole pairs number of DFIG. The stator field is oriented along the d axis of frame. The grid is considered stable and perfect and the stator resistance of DFIG is neglected. Therefore, we can write the (9) and (10).

$$\begin{cases} \psi_{ds} = \psi_s = L_s I_{ds} + M_{sr} I_{dr} \\ \psi_{qs} = 0 = L_s I_{qs} + M_{sr} I_{qr} \end{cases} \quad (9)$$

$$\begin{cases} V_{ds} = 0 \\ V_{qs} = \omega_s \psi_{ds} \end{cases} \quad (10)$$

The electromagnetic torque equation becomes (11).

$$\Gamma_a = -n_p \frac{M_{sr}}{L_s} I_{qr} \psi_s \tag{11}$$

The equations of both powers become (12).

$$\begin{cases} P_s = -\frac{M_{sr}}{L_s} V_s I_{qr} \\ Q_s = -\frac{M_{sr}}{L_s} V_s I_{dr} + V_s \frac{\psi_s}{L_s} \end{cases} \tag{12}$$

Based on (5) and (9) the rotor state equations are expressed as (13),

$$\begin{cases} \dot{I}_{dr} = \frac{1}{L_r \sigma} (-R_r I_{dr} + V_{dr} + s \omega_s L_r \sigma I_{qr}) \\ \dot{I}_{qr} = \frac{1}{L_r \sigma} (-R_r I_{qr} + V_{qr} - s \omega_s L_r \sigma I_{dr} - s \frac{M_{sr} V_s}{L_s}) \end{cases} \tag{13}$$

where $\sigma = 1 - \frac{M_{sr}^2}{L_r L_s}$ and s denote respectively the dispersion coefficient and the slip speed. The block diagram of a simplified DFIG model [24] can be determined by using (11), (12) and (13) and can be described by Figure 3.

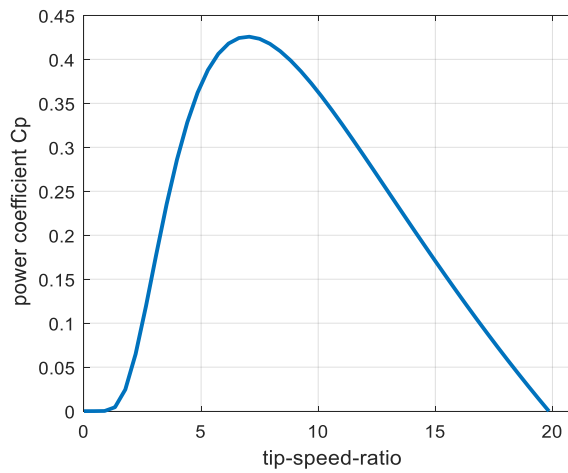


Figure 2. Variation of the power coefficient Cp

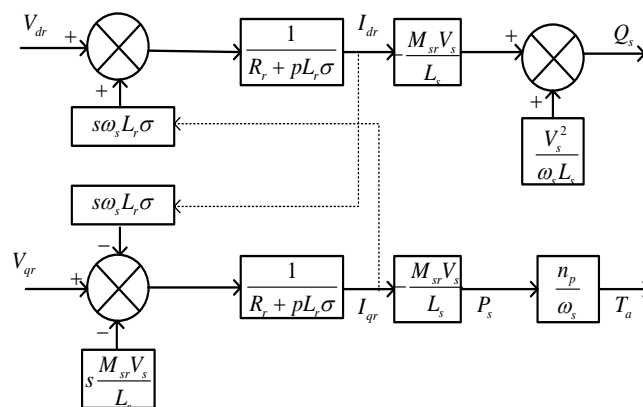


Figure 3. Simplified DFIG model block diagram

3. DFIG CONTROL

The DFIG control chain has two nested loops, one for the current and another for the speed. The internal current loop admits a faster dynamic than that of the speed. Indeed, the quadratic current reference value is deduced from the external velocity loop [25], [26]. The optimal reference speed is deduced from the MPPT characteristic, which describes the evolution of power as a function of turbine speed for different values of wind speed [27].

In this section, we propose two types of current controllers. In the first subsection, we present the classical proportional integral controller. Whereas, in the second subsection a new sliding mode control, which has the same architecture as the proportional-integral controller is designed. In the third and fourth subsections are respectively reserved to the speed controller and the presentation of T-S fuzzy supervisor.

3.1. Current PI controller

The PI controller is used for linear system. In our case, the DFIG is a nonlinear system. However, it is necessary to decouple the variables of the direct and quadrature axes. To appear the transfer functions for both axes, the vector control is achieved by eliminating the coupling terms by compensating the term $(-s\omega_s L_r \sigma I_{qr})$ on the d-axis and the term $(s\omega_s L_r \sigma I_{dr} + s \frac{M_{sr} V_s}{L_s})$ on the q-axis. This allows for each of the axes to be controlled independently of the other with its own PI controller. The procedure for controlling the direct and quadratic rotor currents of the DFIG by the PI controller is similar. Indeed, after decoupling the magnitudes of the two direct and quadratic axes, the current regulation block diagrams are identical. We are content to represent a single loop whose reference and measured quantities are I_{dq} to say that it is valid for the both axes (d and q) as shown in Figure 4. The quadratic reference current can be computed basis on the electromagnetic torque (11). Whereas, reference current along the direct axis is maintained constant to cancel the reactive power according to (12).

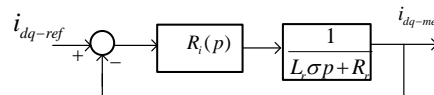


Figure 4. The current loop

The current regulator equation:

$$R_i(p) = K_{ip} + \frac{K_{ii}}{p} \quad (14)$$

The current transfer function:

$$\frac{i_{dq-mes}(p)}{i_{dq-ref}(p)} = \frac{K_{ip}}{L_r \sigma} \frac{p + \frac{K_{ii}}{K_{ip}}}{p^2 + \frac{R_r + K_{ip}}{L_r \sigma} p + \frac{K_{ii}}{L_r \sigma}} \quad (15)$$

The regulation parameters are given by:

$$K_{ip} = 2\xi\omega_i L_r \sigma - R_r \quad (16)$$

$$K_{ii} = L_r \sigma \omega_i^2 \quad (17)$$

The DFIG control block diagram using PI type controller can be illustrated by Figure 5.

3.2. Current sliding mode controller (SMC)

The SMC approach is considered as a robust control. However, to guarantee the convergence of currents errors towards zero for all reference values, we propose in this subsection the development of a controller basis on the theory of sliding modes. The control law includes two components, as shown in the following [28]:

$$u = u_{eq} + u_s$$

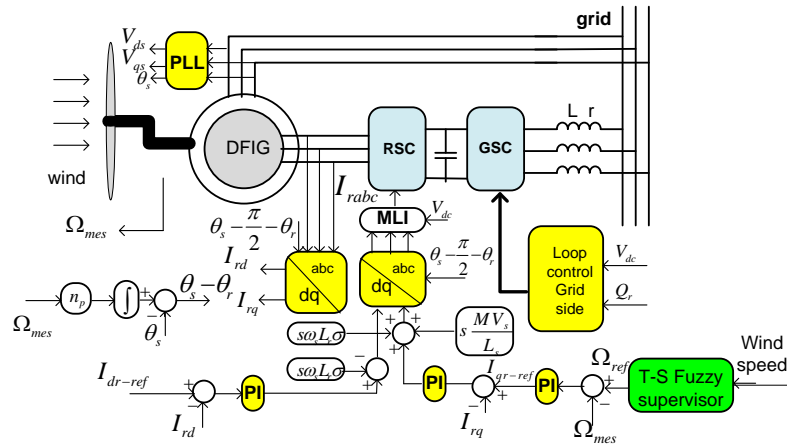


Figure 5. Block diagram of DFIG control using PI regulator

The first one is known as equivalent control term and the second is the switching control term. In the case of DFIG, two surfaces are defined, one for the current along the direct axis and another for the current along the quadrature axis as shown by (18):

$$\begin{cases} s_1 = I_{dr-ref} - I_{dr} + c_1 \int_0^t (I_{dr-ref} - I_{dr}) dt \\ s_2 = I_{qr-ref} - I_{qr} + c_2 \int_0^t (I_{qr-ref} - I_{qr}) dt \end{cases} \quad (18)$$

with c_1 and c_2 are two positive constants. The derivative of the sliding surface gives:

$$\begin{cases} \dot{s}_1 = -\dot{I}_{dr} + c_1 (I_{dr-ref} - I_{dr}) \\ \dot{s}_2 = -\dot{I}_{qr} + c_2 (I_{qr-ref} - I_{qr}) \end{cases} \quad (19)$$

using (13) which gives:

$$\begin{cases} \dot{s}_1 = \frac{R_r}{L_r \sigma} I_{dr} - \frac{V_{dr}}{L_r \sigma} - s \omega_s I_{qr} + c_1 (I_{dr-ref} - I_{dr}) \\ \dot{s}_2 = \frac{R_r}{L_r \sigma} I_{qr} - \frac{V_{qr}}{L_r \sigma} + s \frac{M_{sr} V_s}{L_s L_r \sigma} + s \omega_s I_{dr} + c_2 (I_{qr-ref} - I_{qr}) \end{cases} \quad (20)$$

the equivalent control laws along the direct and quadrature axes V_{dr-eq} and V_{qr-eq} are calculated from $\dot{s}_1 = 0$ and $\dot{s}_2 = 0$ which allows writing:

$$\begin{cases} V_{dr-eq} = (R_r - c_1 L_r \sigma) I_{dr} - s \omega_s L_r \sigma I_{qr} + c_1 L_r \sigma I_{dr-ref} \\ V_{qr-eq} = (R_r - c_2 L_r \sigma) I_{qr} + s \omega_s L_r \sigma I_{dr} + s \frac{M_{sr} V_s}{L_s} + c_2 L_r \sigma I_{qr-ref} \end{cases} \quad (21)$$

in the sliding mode approach the reaching condition, $s_i \dot{s}_i < 0$, must be verified. So, $s_1 \dot{s}_1 < 0$ and $s_2 \dot{s}_2 < 0$ must be verified.

$$\begin{cases} s_1 \dot{s}_1 = s_1 \left(\frac{R_r}{L_r \sigma} I_{dr} - \frac{(V_{dr-eq} + V_{dr-s})}{L_r \sigma} - s \omega_s I_{qr} + c_1 (I_{dr-ref} - I_{dr}) \right) \\ s_2 \dot{s}_2 = s_2 \left(\frac{R_r}{L_r \sigma} I_{qr} - \frac{(V_{qr-eq} + V_{qr-s})}{L_r \sigma} + s \frac{M_{sr} V_s}{L_s L_r \sigma} + s \omega_s I_{dr} + c_2 (I_{qr-ref} - I_{qr}) \right) \end{cases} \quad (22)$$

Basis on (21) the (22) becomes as follow:

$$\begin{cases} s_1 \dot{s}_1 = s_1 \frac{(-V_{dr-s})}{L_r \sigma} \\ s_2 \dot{s}_2 = s_2 \frac{(-V_{qr-s})}{L_r \sigma} \end{cases} \quad (23)$$

if we choose $V_{dr-s} = k_1 \text{sign}(s_1)$ and $V_{qr-s} = k_2 \text{sign}(s_2)$ with $k_1 > 0$ and $k_2 > 0$, the reaching conditions are verified as shown (24).

$$\begin{cases} s_1 \dot{s}_1 = -\frac{s_1 k_1}{L_r \sigma} \text{sign}(s_1) = -K_1 |s_1| < 0 \\ s_2 \dot{s}_2 = -s_2 \frac{s_2 k_2}{L_r \sigma} \text{sign}(s_2) = -K_2 |s_2| < 0 \end{cases} \quad (24)$$

The expressions of the global commands along the direct and quadrature axes are given by:

$$\begin{cases} V_{dr} = V_{dr-eq} + V_{dr-s} = R_r I_{dr} - s \omega_s L_r \sigma I_{qr} + c_1 L_r \sigma (I_{dr-ref} - I_{dr}) + k_1 \text{sign}(s_1) \\ V_{qr} = V_{qr-eq} + V_{qr-s} = R_r I_{qr} + s \omega_s L_r \sigma I_{dr} + s \frac{M_{sr} V_s}{L_s} + c_2 L_r \sigma (I_{qr-ref} - I_{qr}) + k_2 \text{sign}(s_2) \end{cases} \quad (25)$$

the speed regulator provides the quadratic reference current of the rotor while the reference according to the direct axis of rotor is equal to $\frac{\psi_s}{M_{sr}}$ to cancel the reactive power [29]. The block diagram of DFIG control using SMC can be illustrated as follow Figure 6.

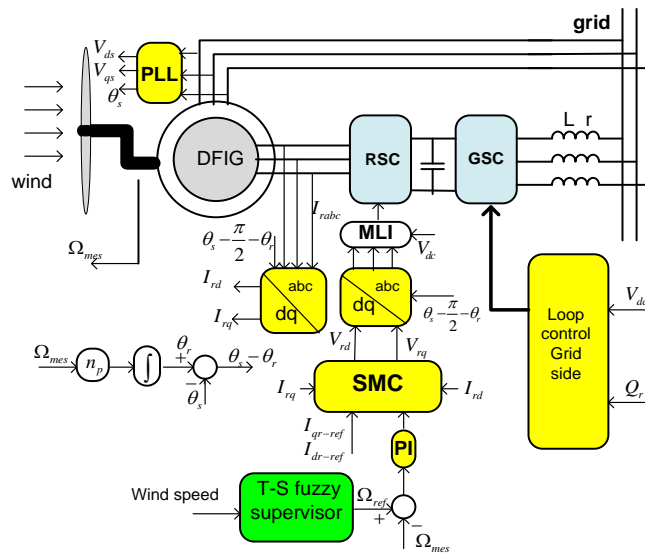


Figure 6. Block diagram of DFIG control using SMC

The dynamics of the current loop is very fast so that it can be neglected in front of that of the speed loop, which makes it possible to trace the speed regulation chain in Figure 7. The speed regulator equation:

$$R_\Omega(p) = k_{p\Omega} + \frac{k_{i\Omega}}{p} \quad (26)$$

The speed transfer function:

$$\frac{\Omega_{mes}(p)}{\Omega_{ref}(p)} = \frac{k_{p\Omega}}{J} \frac{p + \frac{k_{i\Omega}}{k_{p\Omega}}}{p^2 + \frac{(f+k_{p\Omega})}{J}p + \frac{k_{i\Omega}}{J}} \quad (27)$$

Regulation parameters:

$$k_{\Omega p} = 2\xi \omega_\Omega J - f \quad (28)$$

$$k_{\Omega i} = J \omega_\Omega^2 \quad (29)$$

3.4. T-S fuzzy supervisor

Based on knowledge of extreme wind speeds such as (V_{min} , V_{max}) that the turbine can support, as well as the corresponding optimal angular speeds (Ω_{opt1} , Ω_{opt2}) for each of the corresponding wind speeds as

well as the optimal powers provided. However, it is possible to compute, exploiting a T-S fuzzy type supervisor, the optimal velocity Ω_{opt} and the electrical converted power P_{opt} for each wind speed situated in the range (V_{min}, V_{max}) . The membership functions of the T-S fuzzy supervisor are shown by Figure 8.

$$\Omega_{ref} = \Omega_{opt} = M_1 \cdot \Omega_{opt1} + M_2 \cdot \Omega_{opt2} \tag{30}$$

$$P_{ref} = P_{opt} = N_1 P_{opt1} + N_2 P_{opt2} \tag{31}$$

Where, $N_1 = \frac{V^3 - V_{min}^3}{V_{max}^3 - V_{min}^3}$ and $N_2 = \frac{V_{max}^3 - V^3}{V_{max}^3 - V_{min}^3}$ describe the membership functions for converted power. P_{opt1} and P_{opt2} define the optimum powers for the extremes wind speed.

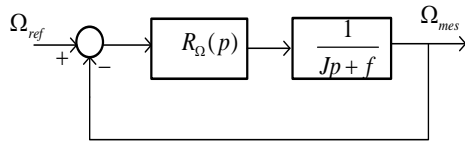


Figure 7. The speed loops

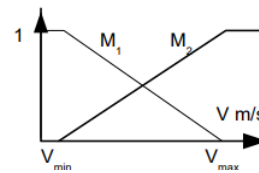


Figure 8. Membership functions for wind

4. SIMULATION RESULTS AND DISCUSSION

To check the performance of the two control techniques: PI control and SMC control, we used MATLAB/Simulink software. The parameters of the DFIG and the turbine are indicated by the Table 1. The wind speed variation is trapezoidal between 6 m/s and 13 m/s to 9 m/s as shown in Figure 9. It gives the DFIG speed variation between 80 rad/s and 170 rad/s to 116 rad/s. The Figures 10 to 15 show respectively speed variation, quadratic and direct rotor currents evolution, three phases rotor currents, stator power variation and the electromagnetic torque variation.

In Figure 10 the speed follows its reference determined by the T-S fuzzy supervisor. According to the Figure 11, Figure 12 and Figure 13, it is noted that the PI control method generates oscillations at the level of the rotor currents, which is not the case for the SMC control method. To avoid the phenomenon of chattering for the control technique by SMC the switching function has been changed by the saturation function and with an adequate choice of its constant k_i . The effect of rotor current oscillations resulting to the PI controller affects both powers injected to the network as shown by Figure 14 and the electromagnetic torque Figure 15.

Table 1. Parameters wind turbine

Value	Parameters	Value	Parameters
2 Mw	DFIG power	2.5 mH	Mutual inductance
0.0026 Ω	Resistance of stator	2	Number of pole pairs
0.0029 Ω	Resistance of rotor	75	Gear reduction ratio
2.587 mH	Inductance of stator	40	Radius of turbine
2.587 mH	Inductance of rotor		

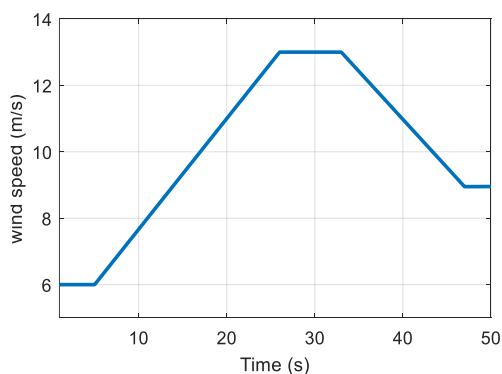


Figure 9. Wind speed variation

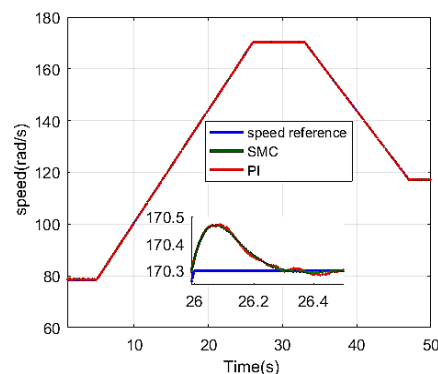


Figure 10. Speed variation

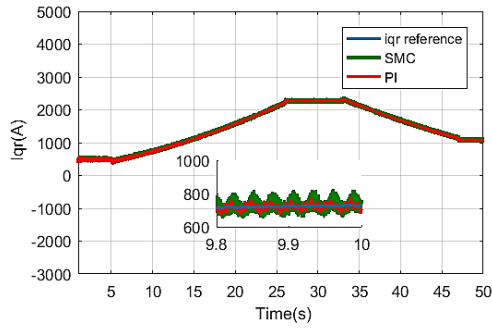


Figure 11. Quadratic rotor current evolution

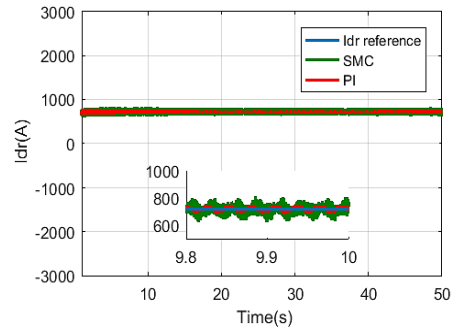


Figure 12. Direct rotor current evolution

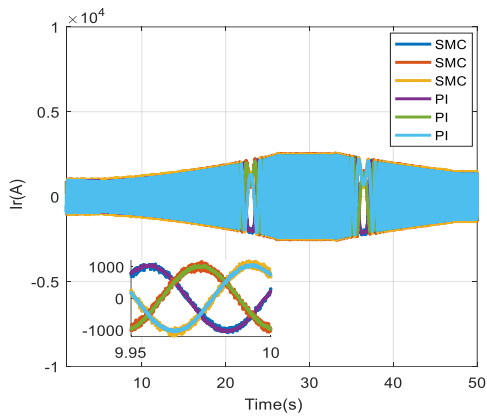


Figure 13. Three phase rotor current

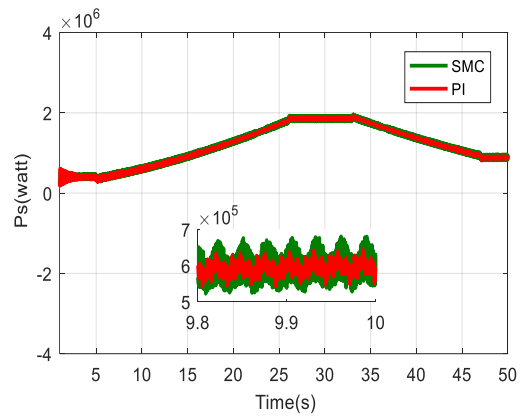


Figure 14. Stator active power variation

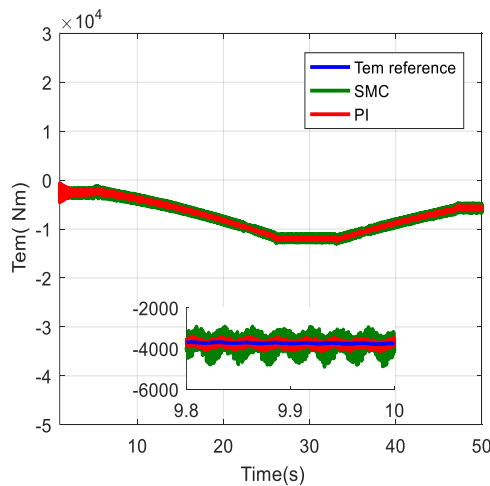


Figure 15. Electromagnetic torque variation

5. CONCLUSION

This paper describes two types of controllers namely the popular classical controller PI and the SMC for a WECS using the DFIG. Although the PI-based control strategy looks simply, it has severe disadvantages that make it ineffective for various applications. In addition, a T-S type fuzzy supervisor is developed to predict the optimal turbine speed and power that it can convert from the wind. The presented simulation results prove that SMC could be an attractive solution for a WECS exploiting the DFIG. However, the chattering phenomenon keep an important problem with this approach. The results demonstrate that the

SMC strategy is more interesting and efficient in terms of maximizing power conversion, compared to the traditional PI technique.




REFERENCES

- [1] H. Abdelli, A. Mezouar, M. Bendjebbar, and K. Belgacem, "Synthesis of smc algorithms applied to wind generator," *International Journal of Power Electronics and Drive Systems*, vol. 12, no. 1, pp. 404–412, 2021, doi: 10.11591/ijpeds.v12.i1.pp404-412.
- [2] G. Abad, J. López, M. A. Rodríguez, L. Marroyo, and G. Iwanski, "Doubly Fed Induction Machine: Modeling and Control for Wind Energy Generation," in *Doubly Fed Induction Machine: Modeling and Control for Wind Energy Generation*, 2011. doi: 10.1002/9781118104965.
- [3] A. Tounsi and H. Abid, "Generator and grid side converter control for wind energy conversion system," *International Journal of Power Electronics and Drive Systems*, vol. 12, no. 3, pp. 1832–1844, 2021, doi: 10.11591/ijpeds.v12.i3.pp1832-1844.
- [4] K. Ouari, T. Rekioua, and M. Ouhrouche, "Nonlinear model predictive controller of a variable speed wind turbine driven doubly fed induction generator," *Journal of Electrical Systems*, vol. 9, no. 2, pp. 243–255, 2013.
- [5] R. Benadli, B. Khiari, and A. Sellami, "Three-phase grid-connected photovoltaic system with maximum power point tracking technique based on voltage-oriented control and using sliding mode controller," *2015 6th International Renewable Energy Congress, IREC 2015*, 2015, doi: 10.1109/IREC.2015.7110963.
- [6] K. Noussi, A. Abouloifa, H. Katir, I. Lachkar, and F. Giri, "Nonlinear control of grid-connected wind energy conversion system without mechanical variables measurements," *International Journal of Power Electronics and Drive Systems*, vol. 12, no. 2, pp. 1139–1149, 2021, doi: 10.11591/ijpeds.v12.i2.pp1139-1149.
- [7] X. Lin, K. Xiahou, Y. Liu, and Q. H. Wu, "Design and Hardware-in-the-Loop Experiment of Multiloop Adaptive Control for DFIG-WT," *IEEE Transactions on Industrial Electronics*, vol. 65, no. 9, pp. 7049–7059, 2018, doi: 10.1109/TIE.2018.2798566.
- [8] R. Mahroug, M. Matallah, and S. Abudura, "Modeling of wind turbine based on dual DFIG generators," *International Journal of Power Electronics and Drive Systems*, vol. 13, no. 2, pp. 1170–1185, 2022, doi: 10.11591/ijpeds.v13.i2.pp1170-1185.
- [9] A. Boyette, "Control-command of a double-fed induction generator with storage system for wind power generation," Université Henri Poincaré-Nancy I, 2006.
- [10] H. Abu-Rub, M. Malinowski, and K. Al-Haddad, "Power Electronics for Renewable Energy Systems, Transportation and Industrial Applications," *Power Electronics for Renewable Energy Systems, Transportation and Industrial Applications*, vol. 9781118634035, pp. 1–795, 2014, doi: 10.1002/9781118755525.
- [11] A. S. L. V. Tummala, "A robust composite wide area control of a DFIG wind energy system for damping inter-area oscillations," *Protection and Control of Modern Power Systems*, vol. 5, no. 1, 2020, doi: 10.1186/s41601-020-00170-y.
- [12] K. M. Haneesh and T. Raghunathan, "Robust Control of DFIG Based Wind Energy System Using an H_∞ Controller," *Journal of Electrical Engineering and Technology*, vol. 16, no. 3, pp. 1693–1707, 2021, doi: 10.1007/s42835-021-00699-4.
- [13] L. L. Rodrigues, J. Sebastian Solis-Chaves, O. A. C. Vilcanqui, and A. J. S. Filho, "Predictive Incremental Vector Control for DFIG with Weighted-Dynamic Objective Constraint-Handling Method-PSO Weighting Matrices Design," *IEEE Access*, vol. 8, pp. 114112–114122, 2020, doi: 10.1109/ACCESS.2020.3003285.
- [14] A. S. L. V. Tummala, "Modified vector controlled DFIG wind energy system based on barrier function adaptive sliding mode control," *Protection and Control of Modern Power Systems*, vol. 4, no. 1, 2019, doi: 10.1186/s41601-019-0119-3.
- [15] M. I. Martinez, G. Tapia, A. Susperregui, and H. Camblong, "Sliding-mode control for DFIG rotor- and grid-side converters under unbalanced and harmonically distorted grid voltage," *IEEE Transactions on Energy Conversion*, vol. 27, no. 2, pp. 328–339, 2012, doi: 10.1109/TEC.2011.2181996.
- [16] S. Boubzizi, H. Abid, A. El hajjaji, and M. Chaabane, "Comparative study of three types of controllers for DFIG in wind energy conversion system," *Protection and Control of Modern Power Systems*, vol. 3, no. 1, 2018, doi: 10.1186/s41601-018-0096-y.
- [17] H. Karimi-Davijani, A. Sheikholeslami, H. Livani, and M. Karimi-Davijani, "Fuzzy Logic Control of Doubly Fed Induction Generator Wind Turbine 1 1," *World Applied Sciences Journal*, vol. 6, no. 4, pp. 499–508, 2009, doi: 10.5281/zenodo.4308924.
- [18] D. Kairous and R. Wamkeue, "DFIG-based fuzzy sliding-mode control of WECS with a flywheel energy storage," *Electric Power Systems Research*, vol. 93, pp. 16–23, 2012, doi: 10.1016/j.epr.2012.07.002.
- [19] A. A. Chhipa *et al.*, "Adaptive neuro-fuzzy inference system-based maximum power tracking controller for variable speed wecs," *Energies*, vol. 14, no. 19, 2021, doi: 10.3390/en14196275.
- [20] Y. Majdoub, A. Abbou, and M. Akherraz, "High-performance MPPT control of DFIG with optimized flux reference in presence of nonlinear magnetic characteristic," *International Journal of Power Electronics and Drive Systems*, vol. 13, no. 2, pp. 1195–1208, 2022, doi: 10.11591/ijpeds.v13.i2.pp1195-1208.
- [21] M. W. K. Mbukani and N. Gule, "PLL-Based Sliding Mode Observer Estimators for Sensorless Control of Rotor-Tied DFIG Systems," *IEEE Transactions on Industry Applications*, vol. 55, no. 6, pp. 5960–5970, 2019.
- [22] B. Beltran, M. E. H. Benbouzid, and T. Ahmed-Ali, "Second-order sliding mode control of a doubly fed induction generator driven wind turbine," *IEEE Transactions on Energy Conversion*, vol. 27, no. 2, pp. 261–269, 2012, doi: 10.1109/TEC.2011.2181515.
- [23] S. Mensou, A. Essadki, T. Nasser, and B. Bououlid Idrissi, "A direct power control of a DFIG based-WECS during symmetrical voltage dips," *Protection and Control of Modern Power Systems*, vol. 5, no. 1, 2020, doi: 10.1186/s41601-019-0148-y.
- [24] M. N. Musarrat and A. Fekih, "A Fault-Tolerant Control Framework for DFIG-Based Wind Energy Conversion Systems in a Hybrid Wind/PV Microgrid," *IEEE Journal of Emerging and Selected Topics in Power Electronics*, vol. 9, no. 6, pp. 7237–7252, Dec. 2021, doi: 10.1109/JESTPE.2020.3034604.
- [25] S. Ghosh, Y. J. Isbeih, R. Bhattarai, M. S. El Moursi, E. F. El-Saadany, and S. Kamalasan, "A Dynamic Coordination Control Architecture for Reactive Power Capability Enhancement of the DFIG-Based Wind Power Generation," *IEEE Transactions on Power Systems*, vol. 35, no. 4, pp. 3051–3064, 2020, doi: 10.1109/TPWRS.2020.2968483.
- [26] S. M. Tripathi, A. N. Tiwari, and D. Singh, "Optimum design of proportional-integral controllers in grid-integrated PMSG-based wind energy conversion system," *International Transactions on Electrical Energy Systems*, vol. 26, no. 5, pp. 1006–1031, 2016, doi: 10.1002/etep.2120.
- [27] H. M. Seoudy, M. A. Saadeldin, and W. A. Mohamed, "Design and implementation of optimal controller for DFIG-WT using autonomous groups particle swarm optimization," *International Journal of Power Electronics and Drive Systems*, vol. 13, no. 3, pp. 1813–1821, 2022, doi: 10.11591/ijpeds.v13.i3.pp1813-1821.




- [28] H. Abid, "Takagi-Sugeno Fuzzy Controller and Sliding Mode Controller for a Nonholonomic Mobile Robot," *Mathematical Problems in Engineering*, vol. 2021, 2021, doi: 10.1155/2021/7703165.
- [29] S. Sharma, J. P. Mishra, and S. Datta, "Sliding mode power control of a DFIG based variable speed wind energy conversion system," *12th IEEE International Conference Electronics, Energy, Environment, Communication, Computer, Control: (E3-C3), INDICON 2015*, 2016, doi: 10.1109/INDICON.2015.7443335.

BIOGRAPHIES OF AUTHORS






Atef Jemmali    obtained the Master degree in automatic, from higher school of sciences and techniques of Tunisia 2009. He is currently member of Laboratory of Sciences and Techniques of Automatic Control and Computer Engineering (Lab-STA) in National School of Engineering of Sfax, University of Sfax, Tunisia. He is currently PhD student in National School of Engineering of Sfax. His research interests include development of control approaches for hybrid renewable energy systems. He can be contacted at email: atefjemmali@gmail.com.






Khaled Elleuch    obtained the M.S degree on January 1996 in electrical engineering from the ESSTT of Tunis, Tunisia. He is member of Laboratory of Sciences and Techniques of Automatic and Computer Engineering (Lab-STA) in National Engineering School of Sfax, University of Sfax. He obtained the Ph.D. degree from National Engineering School of Sfax ENIS, Tunisia on June 2010. Currently, he is an associate professor in the Higher Institute of Biotechnology of Sfax ISBS, Tunisia. His researches focus on identification and control of nonlinear systems, photovoltaic energy and wind energy. He can be contacted at email: Khaled.elleuche@isbs.usf.tn.



Hafedh Abid    had an electrical engineering diploma from the National School of Engineering of Sfax, Tunisia in 1989, then a diploma in Electrical and Electronic from the High School of Technical Sciences of Tunis in 1995 and in 1996 the Aggregation in Electric Genius. From 1996 to 2006, he was a 'Technologies' Teacher of the Electric Department in High Institute of Technologies of Sousse. He is working now as a Professor at National School of Engineering of Sfax, University of Sfax, Tunisia. His current research interests are fuzzy systems and photovoltaic systems. He is the author and co-author of numerous national and international publications. He can be contacted at email: hafedh.abid@enis.tn.



Ahmed Toumi    is an electrical engineer from the Sfax Engineering National School, he has the DEA in instrumentation and Measurement from University of Bordeaux, France in 1981 and the Thesis degree from the University of Tunis in 1985. He joined the National Engineering School as an Associate Professor, since 1981. In 2000, he had the University Habilitation (HDR) from the Engineering School of Sfax, Tunisia. He was working as a director of the Electrical Engineering Department in ENIS. Study and research areas touch modeling, stability of electric machines and electrical networks. He can be contacted at email: ahmed.toumi@enis.tn.